doi:10.20944/preprints202305.1924.v1

Communication

Microstructural Characteristic of NiTi Coating on Graphite Substrate by Plasma Spraying Process

Sneha Samal [1,*], Jakub Zeman [2], Jaromír Kopeček [1] and Petr Šittner [1]

[1] FZU—Institute of Physics of the Czech Academy of Sciences, Na Slovance 1999/2, 182 00 Prague, Czech Republic
[2] Faculty of Electrical Engineering, Czech Technical University in Prague. Prague, Czech Republic
*Correspondence: samal@fzu.cz

Abstract: In this study, $Ni_{50}Ti_{50}$ powder was coated on the surface of graphite substrate (C) by plasma spraying process using a radio frequency inductively coupled plasma reactor. The coating was carried out by using 12- and 9-kW power under Ar atmosphere. The cross-section of coating layers and the surface were examined with SEM, EDX, XRD analysis and microhardness test. The thickness and quality of the coating increased with input power. Many pores were detected in the cross-sectional surface areas. Higher input power caused a better coating layer in NiTi alloy. The hardness of the coating layer decreases with higher input power.

Keywords: NiTi coating; graphite substrate; microstructural; plasma spraying

1. Introduction

NiTi coating has been implemented on the surface of the samples for improving material properties. Different coating techniques were carried out by the powder technology routes for this mechanism. The plasma spraying process was widely used for the coating of materials in various forms from gas welding to metal arc welding and spraying of molten metal or alloy powder on the surface of the substrate [1–3]. Thermal plasma technology opens the door to various branches of powder metallurgy for the improvement of material behavior [4,5]. This technique only solves the issue of surface protection and could be able to recover metals from waste materials [6]. The surface coating is performed at extremely high temperatures, excellent arc stability, low thermal distortion, and high coating speeds [7]. In our previous works, we used plasma technology in spark plasma sintering to produce NiTi alloys under various conditions [8]. The plasma spraying process was carried out for the investigation of the adhesion of the coating layer on the surface of the substrate such as stainless steel [9]. The modified techniques with cooler heads in the plasma spraying may play a role in controlling the proper microstructural of the alloy that is used in the present study to investigate its effect on the resulting coating properties. Argon gas is considered a central gas for creating plasma as well as carrier gas for powder particles feeding into the plasma arc. NiTi alloy is known as the most popular and practical shape memory alloy in engineering, medical and orthopedic applications. NiTi coatings have been used also wear resistance against corrosion, and cavitation erosion resistance for various applications [10–12]. The cavitation erosion resistance of NiTi is much higher than that of the base material. So far various coating methods such as laser, vacuum plasma spraying, high-velocity oxide fuel spraying, and plasma air spraying have emerged as potential ways for NiTi coating [13–15].

In this study, NiTi was coated on the surface of graphite substrate (G280) with the aim of easy separation of the coating layer for microstructural study. Plasma spraying by radio frequency plasma is considered a heat source. NiTi coating was performed in different input power under Ar gas protection. Microstructural changes have been observed and phase analysis was examined. The inner surface quality has been examined as the subject of the graphite substrate and possible contamination from the substrate towards coating layers. The hardness of the coating layer is examined as the function of input power.

2. Materials and Methods

Graphite (G280) is considered the substrate for spraying NiTi powder by using a plasma spraying process. The dimensions of the substrate of 60 × 20 × 3 mm were chosen. The thick coating of NiTi was deposited by using a radio frequency inductively coupled plasma (RF-ICP) facility from the Institute of Plasma Physics (IPP), Prague. Table 1 represents the various experimental parameters for the spraying process.

Table 1. Spraying parameters for sample preparation on graphite substrate[1].

Sample	Torch power (kW)	Feeding rate (g/min)	Preheat time (s)	Spraying set up plan	Net powder spray time (s)
1	12	2.1	60	30 × 6	180
2	12	4.2	60	30 x 6	180
3	9	2.1	60	30 x 6	180
4	9	4.2	60	30 x 6	180

[1] Holder is cooled type, Sample X-position <-20: 40>. (mm), stand-off distance: 70 mm, Central and carrier gas : Ar, (10, 8 ml/min), Substrate graphite(G280).

NiTi powder (50:50) with a purity 99.5 % was purchased from American Elements MERELEX CORPORATION, LOS ANGELES, CA 90024, USA for the coating. The elemental composition of the Ni:Ti powders was 50:50 (atom %). NiTi particles are spherical in shape and size. **Figure** 1 (a-c) displays the image of NiTi powder and elemental composition.

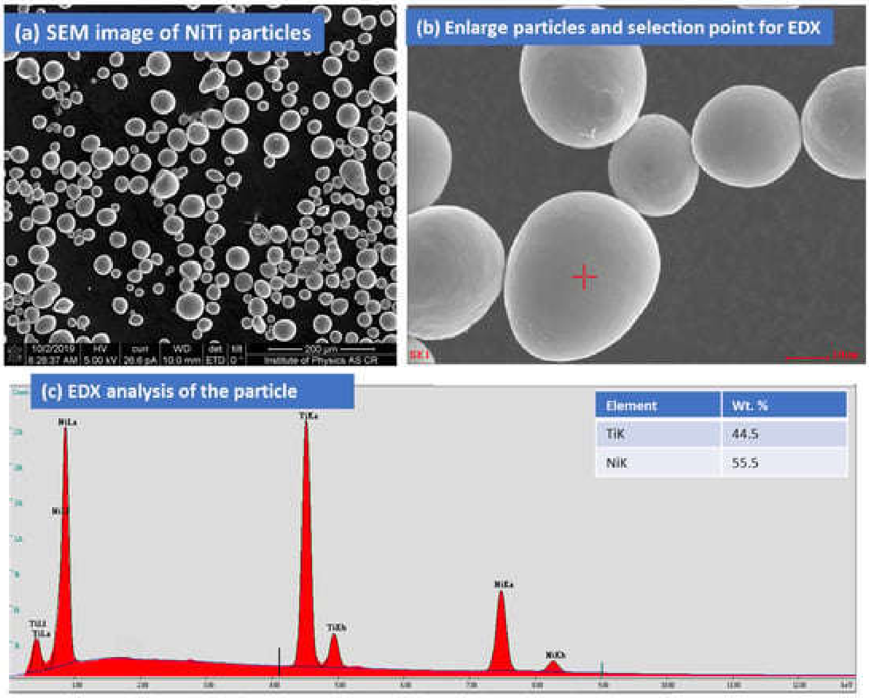

Figure 1. (a,b) Surface image of NiTi particles. (c) EDX analysis of the particle and element composition in wt % (inset) [9].

NiTi powders were inserted into the plasma arc by the powder feeder using various feeding rates (2.1, 4.2 g/min) that allow the impact of molten particles on the graphite substrate to form the coatings. Spraying was performed in six steps that allow the formation of thick coating layers on the graphite substrate. The plasma power and feeding rate control the extent of melting into fully or partially melted splat to impact the substrate. Metallographic examination of the coated layers was performed by initially grinding the substrate of graphite for separation with followed grinding and polishing to 1 µm diamond paste. The scanning electron microscope image was observed by scanning electron microscope (SEM, Tescan FERA 3 (Tescan, Brno, Czech Republic)). The images were investigated by both modes of observation using secondary electrons and backscattered electrons. Energy-dispersive X-ray spectroscopy (EDS) was carried out using the EDAX system (EDAX, Ametek Inc., Mahwah, NJ, USA) with an Octane Super 60 mm^2 detector to determine the chemical composition from substrate towards coating. The phase analysis of the coating layers was detected at room temperature with an X'Pert PRO θ-θ powder diffractometer using Bragg–Brentano geometry at 40 mA and 35 kV with CoKα radiation (average wavelength λ = 0.1790 nm), a focus-slit distance of 100 mm, and a goniometer radius of 240 mm. The data were measured in the 2θ range of 20–120°, using a step size of 0.013°, a scan step time of 1.4 s, and a fixed divergence slit size of 0.5°. The phase transformation temperatures of coating layers were carried out by differential scanning calorimetry (DSC 25, TA Instruments, New Castle, DE, USA) at a heating and cooling rate of 5 °C/min in the temperature range of −50 to +150 °C in a nitrogen environment inside the sample chamber. The shape memory behaviour of the coating is investigated by Thermo-mechanical analysis in bending mode with a static load of 100 mN from −50 to +150 °C in the temperature cycle. The microhardness of the coating on the surface and cross-section was investigated by a Vickers hardness tester for a force of 1.961 N for a duration of 10 s.

3. Results and discussion

The characterization of coatings was investigated in terms of microstructural analysis, the thermal transformation of the phases in the materials, and mechanical deformation as a function of thermal cycles to understand the behavior of shape memory effect as functional properties.

3.1. Microstructural investigation on coatings

The quality of the coating is investigated by observing the cross-section image of various layers and the surface of the samples. Samples were carefully ground and polished effectively to avoid any contamination from the substrate toward the coating layers. **Figure** 2 (a-c) displays sample 1 microstructure in cross-section image and flat surface image. The cross-section view shows some areas of porosity and carbon element contamination. The surface area shows the presence of micropores in the samples. The sample looks good with minor contamination. However, sample 2 shows more contamination in comparison to sample 1. **Figure** 3 (a-c) shows the cross-sectional and surface view of the sample. The presence of carbon elements is visible throughout the thickness. The surface of sample 2 looks fine with some minor contamination of carbon elements. **Figure** 4 shows the microstructure image of sample 3 in cross-sectional and surface view. The cross-section and surface of the sample look extensively contaminated by carbon particles that migrate from the substrate toward the coating layers. The sample is prepared with the condition of low input power and low feed rate, which may allow more interparticle space for the diffusion of carbon elements. Based on the severe contamination of the sample will not be considered for further study. The effect of input power 9 kW partially reflects molten particles in the plasma source, which is confirmed by the layer of porosity that is generated between the layers of the coating. The porosity layer arises from the deadhesion of partially melted splat or unmelted particles within the coating layers. This sample is visible like a net structure which may be beneficial for the researcher material with layers of porosity for application in biomedical uses. As in this work, we are more concerned with the compact sample that could reflect the behavior of thermal and thermo-mechanical behavior.

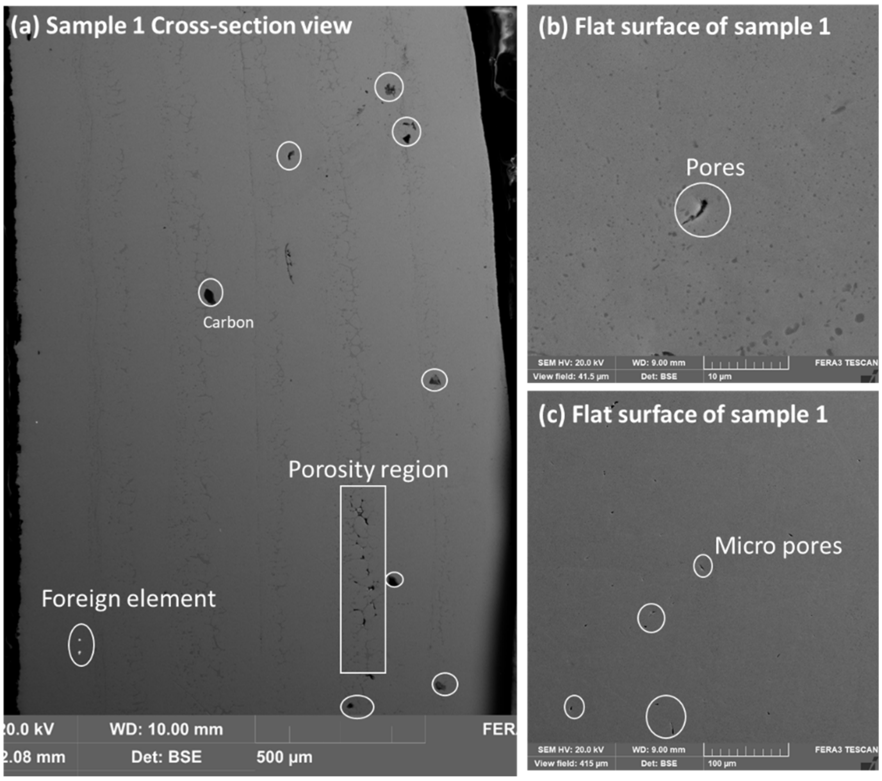

Figure 2. (a-c) Microstructural image of sample 1 (a) cross-section area (b-c) flat surfaces in BSE image mode.

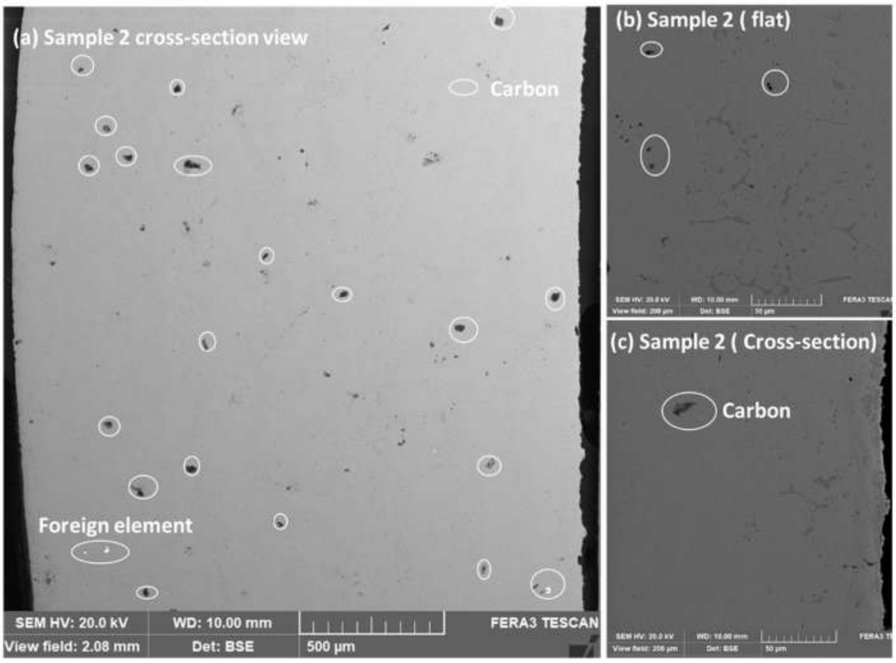

Figure 3. Microstructural image of sample 2, (a) cross-section area (b) flat surface in BSE image mode (c) Cross-section near edge.

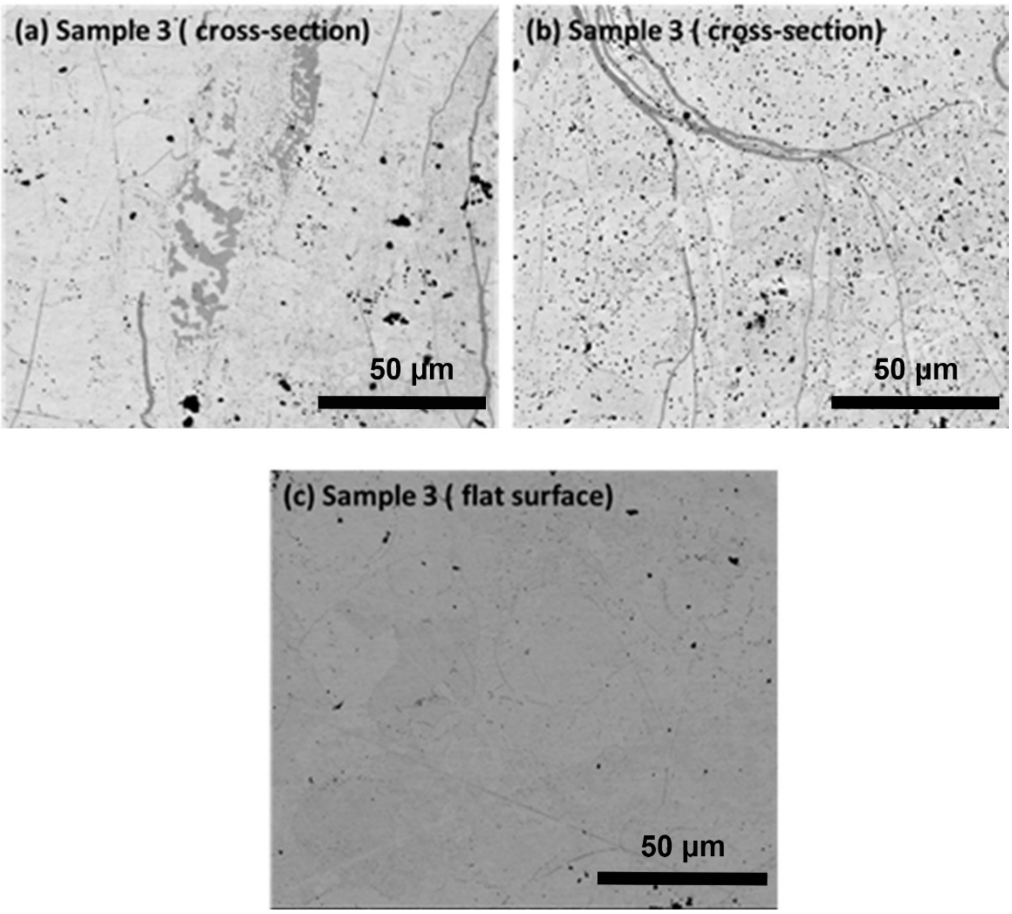

Figure 4. Microstructural image of sample 3, (a) cross-section area (b) cross-section area in BSE image mode (c) flat surface shows more contamination from carbon and phase separation.

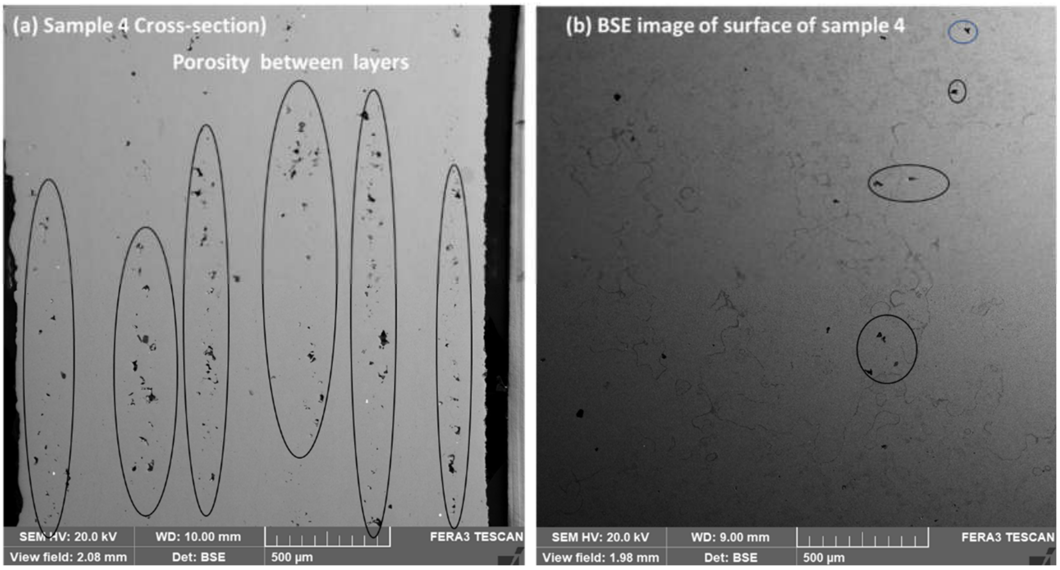

Figure 5. (a) Cross-section image of sample 4 shows porosity at the joining layers throughout the cross-section (b) Surface image of sample 4.

3.2. Phase identification

To understand more depth of the phase analysis, XRD findings are summarized for samples 1 and 2, in Figure 6 (a,b).

Sample 1 shows NiTi phases of martensite (monoclinic, 54.7 %), austenite (cubic, 39.9 %), and oxide phases (Ti4Ni2O, 5.4 %), cubic phases, whereas sample 2 shows presence of intermetallic element with more phases of NiTi such as martensite (monoclinic, 36.9 %), austenite (cubic, 47.2 %), Ni_4Ti_3 (rhombohedral, R-3, 5.7 %) and hexagonal phase of Ti element (5 %) with some oxide phases (Ti_4Ni_2O, 5.2 %).

(a) Sample 1

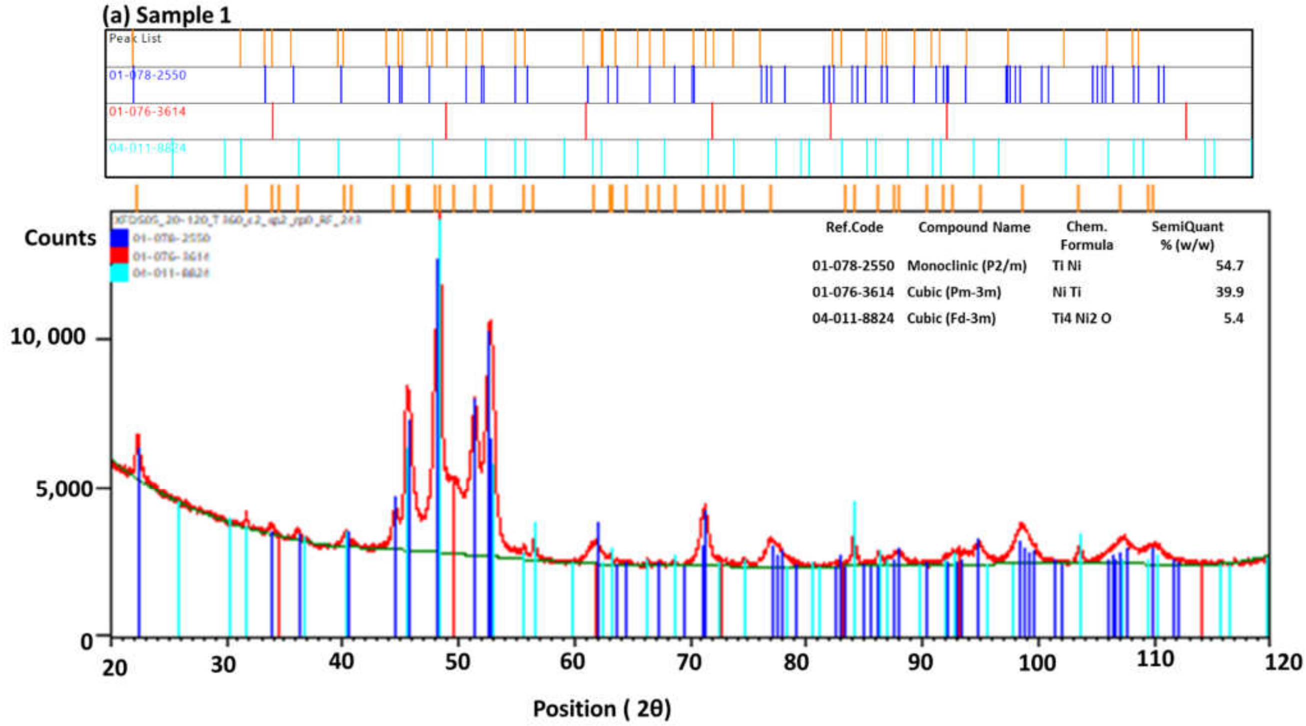

Ref.Code	Compound Name	Chem. Formula	SemiQuant % (w/w)
01-078-2550	Monoclinic (P2/m)	Ti Ni	54.7
01-076-3614	Cubic (Pm-3m)	Ni Ti	39.9
04-011-8824	Cubic (Fd-3m)	Ti4 Ni2 O	5.4

(b) Sample 2

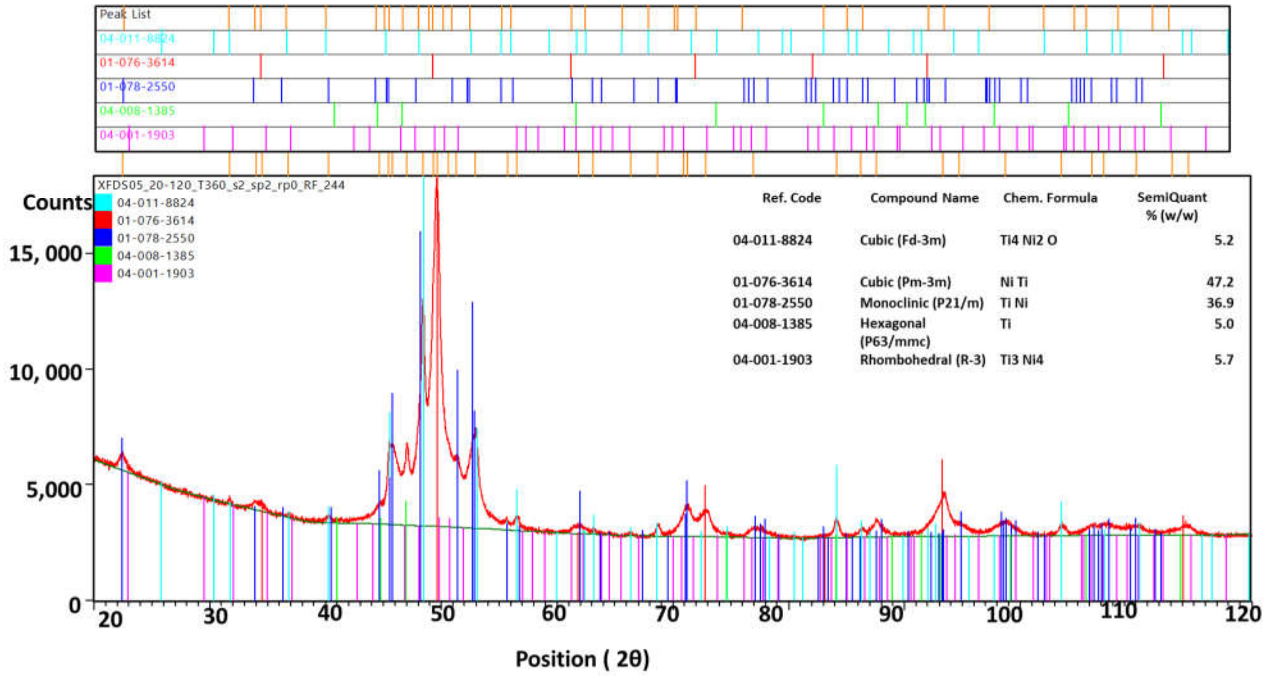

Ref. Code	Compound Name	Chem. Formula	SemiQuant % (w/w)
04-011-8824	Cubic (Fd-3m)	Ti4 Ni2 O	5.2
01-076-3614	Cubic (Pm-3m)	Ni Ti	47.2
01-078-2550	Monoclinic (P21/m)	Ti Ni	36.9
04-008-1385	Hexagonal (P63/mmc)	Ti	5.0
04-001-1903	Rhombohedral (R-3)	Ti3 Ni4	5.7

Figure 6. (a-b) XRD peaks for phase detection for samples 1 and 2 show the austenite, martensite, oxide, and intermetallic phases.

3.3. Thermal characterization of samples

Thermal analysis of samples 1 and 2 reveals the transformation temperature of NiTi phases in cooling and heating cycles. Both samples show strong peaks of martensite and austenite phases, with start and finish temperatures coincides with each other. Sample 2 shows shift in peak position for both phases in the thermal cycle. The austenite peak for sample 2 shows 89.21 °C, whereas sample 1 shows peak position at 93.5 °C. Both the samples show austenite start temperature (A_s) at 74.0 °C, and austenite finish temperature at 102.1 °C. Similarly, both samples show martensite start temperature at 75.3 °C, with martensite finish temperature 42.9 °C. However, sample 2 shows martensite peak at 56.3 °C and sample 1 shows at 59.3 °C. The shift in transformation temperature strongly correlates with finings of phases martensite phase detected by XRD. As the semiquantitative phases of martensite are more in sample 1 compared to sample 2, in cooling cycle, martensite peak arises at lower temperature. The same phenomena are applicable to sample 2 with the dominant austenite phase, shows austenite peak earlier than sample 1. This may correspond to the presence of intermetallic phases in sample 2.

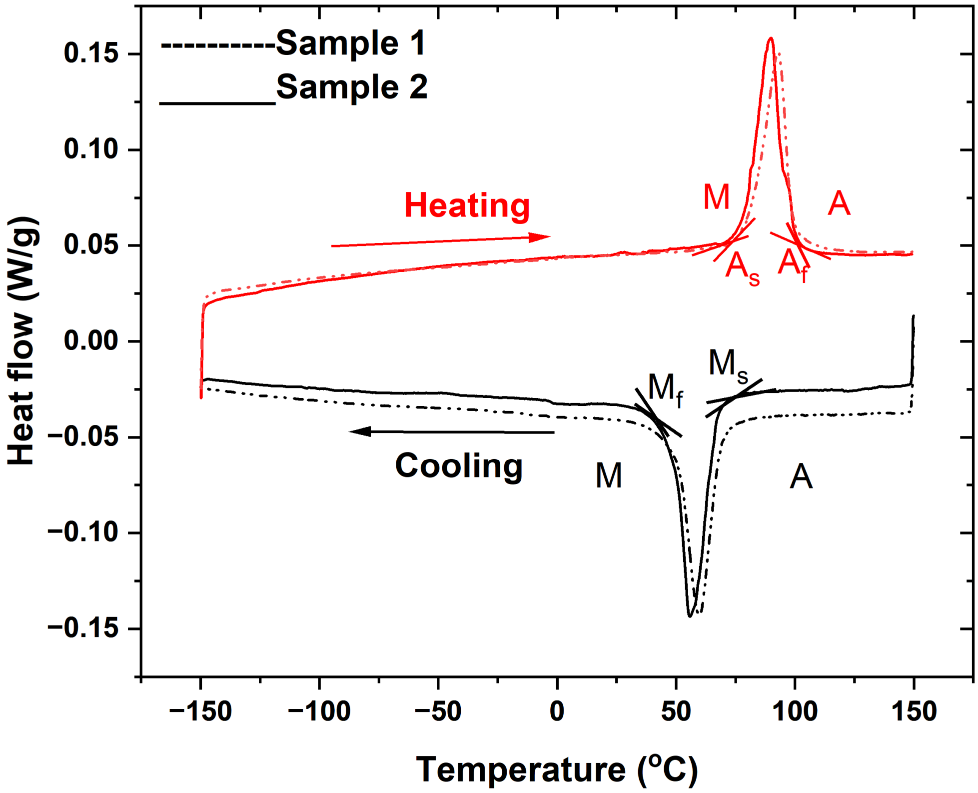

Figure 7. DSC peaks of martensite and austenite phases in samples 1 and 2 show transformation temperature in the cooling and heating cycle.

3.4. Thermo-Mechanical characterization of the sample

Mechanical response of the sample at a constant load of 100 mN is performed as the function of thermal cycles. The sample shows deformation as the change in displacement from the horizontal position to the deformed bend position, the sample returns to the original position after heating back. Figure 8 represents the behavior of samples 1 and 2 as the function of time, displacement (delta), and temperature. Sample 2 has shown more deformation of change in displacement – 45 µm, however sample 1 shows deformation in the range of – 10 µm. Both samples are back to their original position after heating, however, sample 2 shows the slight deviation of – 5 µm displacement from the original position. This deviation may arise due to the presence of contaminations such as carbon elements or other intermetallic phases.

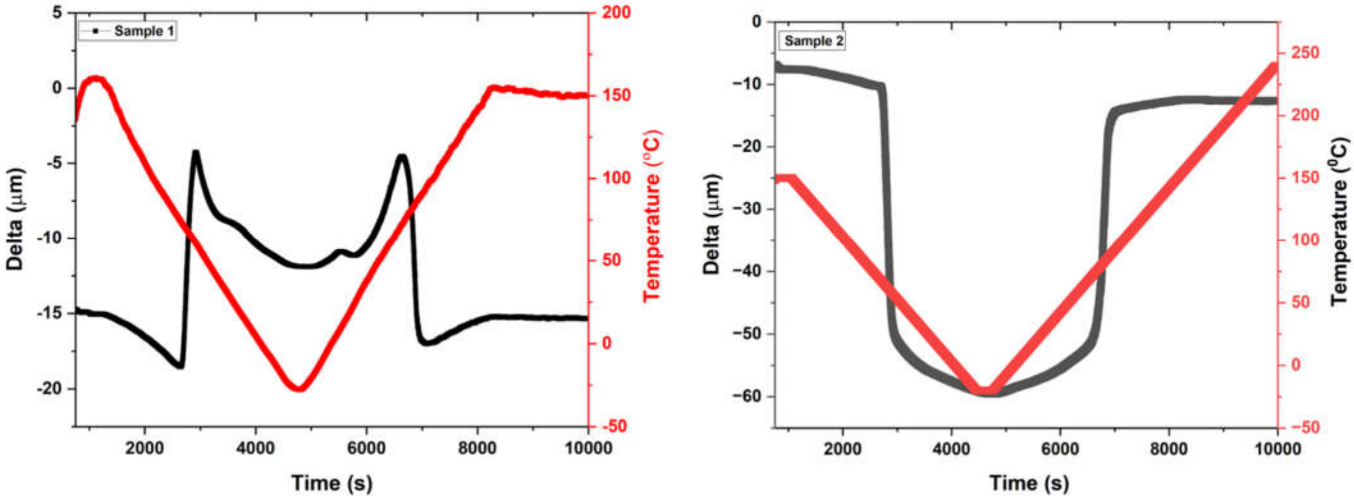

Figure 8. Thermo mechanical analysis of samples 1 and 2 as the function of time, temperature, and displacement (delta).

3.5. Hardness Evaluation

Three selected coatings 1, 2, and 4 have been chosen for hardness test at the cross-section and surface of the samples. **Figure** 9 displays the hardness of the samples with the statistical distribution. Five indents were carried out at the cross section and the surface of the samples for calculation of average and deviation of hardness.

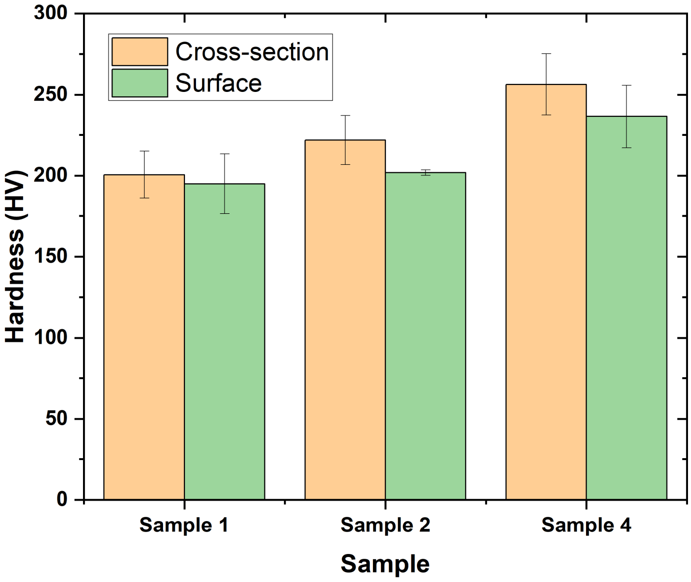

Figure 9. Hardness of samples at cross section and surface area.

The sample shows lower hardness in comparison to the other two samples. This may arise due to better quality of coating in samples with very minor contamination from carbon elements. Sample 4 shows layers of porosity, unmelted sample, and contamination within the structure that may lead to higher hardness.

4. Discussion

The alloy fabricated on the graphite substrate contains carbon on the surface and through the thickness. Carbon as a coating on the surface of alloy provides an advantage against corrosion as the best corrosion resistance **[16–18]**. However, carbon as an element inside the core of the material is considered a contamination or foreign element. However, if the addition of 0.03 Wt. % of C in the form of a compound such as TiC could be inherited as an advantage for an increase in tensile strength and tensile fatigue life [19]. However, if the content of carbon is increased from 0.03 % to 0.05 wt. %, then the material's properties start to deteriorate. In this work, plasma spraying was used to prepare NiTi alloys which are sensitive toward the composition because of the advantage of controlling uniform composition with a multilayer structure. Meanwhile, graphite substrate was chosen because it's cheap and easy to separate by mechanical grinding **[20,21]**. However, the graphite substrate could serve as a source of C that reacts with Ti in the NiTi matrix to produce TiC, which affects the composition ratio of Ni/Ti and thus affects the alloy properties.

Figure 7. estimated martensitic transformation in both samples has a slight variation that may arise due to compositional changes in both samples 1, 2. The shifting of martensite temperature corresponds to Ni concentration in the sample. Sample 1 shows Ni-rich in concentration from the phase analysis of **Figure** 6. There are two potential sources of error that can affect compositional changes. It may occur from the small error associated with the purity of raw material or microstructural constituents that affects Ni concentration in the Ni matrix. Oxygen and carbon emerged as impurities partly through raw material and partly through the fabrication process such as the cooling process of sample preparation and from the graphite substrate respectively. During the thermal plasma fabrication process oxygen and carbon could precipitate out in the matrix of the product as Ti_2NiO_x and TiC components. **Figure** 6 shows that the Ni-rich NiTi alloys contain a small number of oxygens stabilized as Ti2Ni, which reduces the Ti concentration of the matrix. As a result, alloys with higher oxygen content have lower phase transition temperatures.

4.1. Purity of Powder NiTi as raw material

In pure powder such as NiTi alloy, the Ni concentrations in weight percent are expressed as

$$\boldsymbol{C_{Ni}} = \boldsymbol{m_{Ni}}/(\boldsymbol{m_{Ni}} + \boldsymbol{m_{Ti}}) \cdot 100\ \% \qquad \text{---------------------------}(1)$$

where mNi and mTi are the masses of Ni and Ti in the alloys. However, if the raw powder contains some impurities, it affects the final composition. The purity of Ni is P_{Ni} = 99.989 wt. % and Ti is P_{Ti} = 99. 927 wt. % [23]. Considering there is no weight loss during plasma spraying, these purities could able to use the Ni/Ti ratio in the alloy

$$c^{p}_{Ni} = P_{Ni} \cdot m_{Ni}/(P_{Ni} \cdot m_{Ni} + P_{Ti} \cdot m_{Ti}) \cdot 100\ \% \qquad \text{------------------------}\ (2)$$

c^{p}_{Ni} is the purity correction factor. The raw materials used in the present study Ni percentage is used as 50 at. %.

4.2. Role of oxygen and carbon in NiTi alloy

The ternary Ni-Ti-O systém of phase digram is presented in Figure 10 at 1173 K. The diagram highlights various phases of NiTi at 50. % Ni as NiTi phase, with variation in concentration of 30 % Ni as Ti_2 Ni phase. It is particularly noteworthy that Ti_2Ni can dissolve up to 15 at.% oxygen [25].

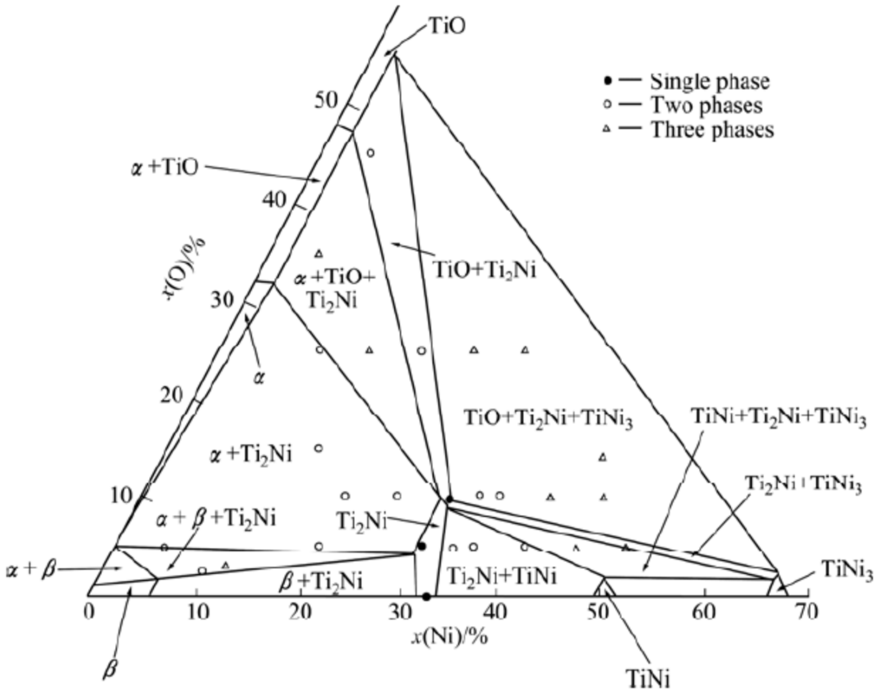

Figure 10. Ni-Ti-O systém for the phase diagram at 1173 K by Rostoker [24].

The phase diagram shows the presence of various phases of $TiO+Ti_2Ni+TiNi_3$ at 1173 K The cooling process may lead to the separation of Ti and Ni phase from the matrix and combines with oxygen for the formation of phases. However, the solubility of O in the Ti_2Ni phase is much lower in **Figure** 6.

5. Conclusions

NiTi alloy was coated on a graphite substrate to consider as standalone material by the plasma spraying process. The following results were achieved:

The effective coating layers of 1.5 mm and 2 mm were obtained for 12- and 9-kW input power respectively. The sample was prepared at higher input power and lower feeding rate showing very minor contamination with good quality microstructure. Although graphite is considered a convenient way, easily removed after spraying, however the source of contamination from the substrate towards the coating by diffusion is more possible. As the carbon content increases the hardness and porosity within the material which is observed in sample 4. Otherwise, controlled spraying parameters at high input power (12 kW) will allow the melting of particles with a lower feeding rate (2.1 g/min) to generate a better sample. The samples prepared at higher power displays significant thermal, and mechanical behavior that corresponds to the shape memory behavior of NiTi alloy.

Author Contributions: “Conceptualization, S.S. and J.K.; methodology, S.S., J.K.; investigation, J.K.; resources, S.S.; writing—original draft preparation, S.S. and J.K.; writing—review and editing.

Funding: Czech Science Foundation (CSF) projects 20-14114S (P. Šittner), Project Solid-21 for the support within the Institute of Physics, Prague, Czech Republic (SOLID21: CZ.02.1.01/0.0/0.0/16_019/0000760, SOLID21-Fyzika pevných látek pro 21. Století, Fyzikální ústav AV ČR, v. v. i. (2018–2023). CzechNanoLab project LM2023051 funded by MEYS CR.

Institutional Review Board Statement: Not applicable.

Informed Consent Statement: Not applicable.

Data Availability Statement: Data will be available at the readers’ request.

Acknowledgments: The first author would like to acknowledge the Institute of Plasma Physics (IPP) of the Czech Academy of Science for the plasma facilities used to prepare samples. The first author would thank Dr. Jana Cibulková, Central Laboratories, University of Chemistry and Technology, Prague (UCT Prague), 166 28 Prague, Czech Republic for XRD analysis.

Conflicts of Interest: The authors declare no conflict of interest.

References

1. Appiah, A.N.S.; Bialas, O.; Czupryński, A.; Adamiak, M. Powder Plasma Transferred Arc Welding of Ni-Si-B+60 wt%WC and Ni-Cr-Si-B+45 wt%WC for Surface Cladding of Structural Steel. *Materials* **2022**, *15*, 4956. https://doi.org/10.3390/ma15144956
2. Trinh, N.Q.; Tashiro, S.; Suga, T.; Kakizaki, T.; Yamazaki, K.; Lersvanichkool, A.; Bui, H.V.; Tanaka, M. Metal Transfer Behavior of Metal-Cored Arc Welding in Pure Argon Shielding Gas. *Metals* **2022**, *12*, 1577. https://doi.org/10.3390/met12101577
3. Heimann, R.B. The Nature of Plasma Spraying. *Coatings* **2023**, *13*, 622. https://doi.org/10.3390/coatings13030622
4. Samal, S. Thermal plasma technology: The prospective future in material processing. J. Clean. Prod. **2017**, 142, 3131–3150.
5. Samal, S. Thermal Plasma Processing of Materials: High-Temperature Applications; Elsevier: Amsterdam, The Netherlands, 2022; pp. 512–525.
6. Samal, S.; Blanco, I. An Overview of Thermal Plasma Arc Systems for Treatment of Various Wastes in Recovery of Metals. Materials **2022**, 15, 683.
7. Samal, S.; Tyc, O.; Cizek, J.; Klecka, J.; Lukáč, F.; Molnárová, O.; de Prado, E.; Weiss, Z.; Kopeček, J.; Heller, L.; et al. Fabrication of Thermal Plasma Sprayed NiTi Coatings Possessing Functional Properties. Coatings **2021**, 11, 610.
8. Samal, S.; Molnárová, O.; Průša, F.; Kopeček, J.; Heller, L.; Šittner, P.; Škodová, M.; Abate, L.; Blanco, I. Net-Shape NiTi Shape Memory Alloy by Spark Plasma Sintering Method. Appl. Sci. **2021**, 11, 1802.
9. Samal, S.; Kopeček, J.; Šittner, P. Interfacial Adhesion of Thick NiTi Coating on Substrate Stainless Steel. *Materials* **2022**, *15*, 8598. https://doi.org/10.3390/ma15238598
10. Samal, S.; Tomáštík, J.; Čtvrtlík, R.; Václavek, L.; Molnárová, O.; Šittner, P. Surface Deformation Recovery by Thermal Annealing of Thermal Plasma Sprayed Shape Memory NiTi Alloys. *Coatings* **2023**, *13*, 433. https://doi.org/10.3390/coatings13020433
11. Samal, S.; Cibulková, J.; Čtvrtlík, R.; Tomáštík, J.; Václavek, L.; Kopeček, J.; Šittner, P. Tribological Behavior of NiTi Alloy Produced by Spark Plasma Sintering Method. *Coatings* **2021**, *11*, 1246. https://doi.org/10.3390/coatings11101246
12. Arciniegas, A.; Casals, J.; Manero Pena, J.; Gil, F.J. Study of hardness and wear behaviour of NiTi shape memory alloys. J. Alloy. Compo. **2008**, 460, 213–219.
13. Chiu K.Y., Cheng F.T., Man H.C., Mater. Sci. Eng., A Struct. Mater.: Prop. Microstruct. Process., 402 (2005), p. 126.
14. Bram M., Ahmad-Khanlou A., Buchkremer H.P., Stöver D., Mater. Lett., 57 (2002), p. 647
15. Serkan Ozel, Bulent Kurt, Ilyas Somunkiran, Nuri Orhan, Microstructural characteristic of NiTi coating on stainless steel by plasma transferred arc process, Surface and Coatings Technology, Volume 202, Issue 15, 2008, Pages 3633-3637, ISSN 0257-8972, https://doi.org/10.1016/j.surfcoat.2008.01.006.
16. Jinbin Zou, Xingyao Wang, Peng Zhang, Xusheng Du, Ultrafast flame coating of carbon and chemical vapor deposition of graphene on NiTi alloy to enhance its corrosion resistance, Diamond and Related Materials, Volume 128, 2022, 109231, ISSN 0925-9635, https://doi.org/10.1016/j.diamond.2022.109231.
17. A. Shanaghi, P.K. Chu, A.R. Sabour Rouhaghdam, R. Xu, T. Hu, Structure and corrosion resistance of Ti/TiC coatings fabricated by plasma immersion ion implantation and deposition on nickel–titanium, Surf. Coat. Technol., 229 (2013), pp. 151-155.
18. Y.-L. Pei, Y. Luan, Surface modification of NiTi alloys using nitrogen doped diamond-like carbon coating fabricated by plasma immersion ion implantation and deposition, J. Alloys Compd., 581 (2013), pp. 873-876.
19. Yang Zhao, Zunyue Yu, Qianyu Wang, Beibei Zhang, Xuepeng Ren, Wenru Zhao, Shubin Ren, Xuanhui Qu, Effect of carbon addition on the microstructure and mechanical behavior of near equiatomic NiTi alloy wire, Materials & Design,

20. Volume 225, 2023, 111570, ISSN 0264-1275,https://doi.org/10.1016/j.matdes.2022.111570.
21. F. Chen, Y.X. Tong, X.L. Lu, X. Wang, B. Tian, L. Li, Effect of graphite addition on martensitic transformation and damping behavior of NiTi shape memory alloy, Mater. Lett., 65 (7) (2011), pp. 1073-1075,
22. Z.H. Zhang, J. Frenzel, K. Neuking, G. Eggeler, On the reaction between NiTi melts and crucible graphite during vacuum induction melting of NiTi shape memory alloys, Acta Mater., 53 (2005), pp. 3971-3985.
23. Z. Zhang, J. Frenzel, C. Somsen, J. Pesicka, K. Neuking, G. Eggeler, Orientation relationship between TiC carbides and B2 phase in as-cast and heat-treated NiTi shape memory alloys, Mater. Sci. Eng. A, 438 (11) (2006), pp. 879-882.
24. Frenzel., J et al., Influence of Ni on martensitic phase transformations in NiTi shape memory alloys, Acta Materialia 58 (2010), 3444-3458.
25. ROSTOKER W. Selected isothermal sections in the titanium-rich corners of the systems Ti-Fe-O, Ti-Cr-O and Ti-Ni-O [J]. Transactions of the Metallurgical Society of AIME 203, 1955(7): 113í116.
26. Ai-Tao QIU, et al., Calculation of phase diagram of Ti-Ni-O systém and application to deoxidation of TiNi alloy, Trans. Nonferrous Met. Soc. China 21 (2011) 1808-1816.